

# Magic Traps for Multiple Rotational States of NaRb Molecule

Svetlana Kotochigova,<sup>1,\*</sup> Qingze Guan,<sup>1,2</sup> Vito Scarola,<sup>3</sup> Brian DeMarco,<sup>4</sup> and Bryce Gadway<sup>4</sup>

<sup>1</sup>*Department of Physics, Temple University, Philadelphia, Pennsylvania 19122, USA*

<sup>2</sup>*Department of Physics and Astronomy, Washington State University, Pullman, Washington 99164-2814, USA*

<sup>3</sup>*Department of Physics, Virginia Tech, Blacksburg, Virginia 24061, USA*

<sup>4</sup>*Department of Physics and IQUIST, University of Illinois at Urbana-Champaign, Urbana, IL 61801-3080, USA*

(Dated: November 6, 2023)

Molecules have vibrational, rotational, spin-orbit and hyperfine degrees of freedom, each of which responds in a unique fashion to external electromagnetic radiation. The coherent control over superpositions of these quantum states is key to manipulation of molecules. For example, the better the coherence time the longer quantum simulations can last. The important quantity for controlling a molecule with laser light is its complex-valued molecular dynamic polarizability. Its real part determines the tweezer potential as felt by the molecule, while its imaginary part contributes to the coherence time. Our studies show that efficient trapping of a molecule in an optical potential can be achieved by a selecting laser frequency that has a small detuning (on the order of tens of GHz) relative to an electric-dipole-forbidden molecular transition. Close proximity to this transition allows us to significantly modify the trapping potentials for multiple rotational states without sacrificing coherences among these states. We demonstrate that magic trapping conditions for multiple rotational states in ultracold  $^{23}\text{Na}^{87}\text{Rb}$  polar molecule can be created. In addition, we show that spin-decoupled magic trapping can be achieved with an applied static electric field oriented along the magnetic field direction.

## I. INTRODUCTION

Optical tweezers and lattices are convenient experimental tools to trap ultracold molecules, but their role in perturbing molecular internal states needs to be understood and managed. To preserve, for example, a superposition of states within the ground electronic potential, optical tweezers must apply the same force to each of these states by creating a so-called magic condition. For polar diatomic molecules trapped in tweezer potentials one of the natural choices for building quantum computer is to store qubits in rotational levels of the ground vibrational states. However, the aspect of engineering traps that support the confinement and long coherence times of molecular rotational levels in the ground state potentials remain challenging. Therefore, it is crucial to develop theoretical models for creating a practical, optimized molecule-based quantum computer.

Molecules offer possibilities not available in other systems. This stems largely from the rich structure of molecular vibrations, rotations, and hyperfine states as well as a non-negligible permanent electric dipole moment for heteronuclear molecules. This dipole moment leads to strong coupling to microwave radiation and static electric fields as well as tuneable long-range electric dipole-dipole interactions between molecules. One of the key challenges for molecule-based quantum science is to engineer optical traps for the molecules to minimize the reduction of their rotational coherence lifetimes due to the trapping lasers, therefore enabling us to exploit the rotational degree of freedom as the quantum bit in quantum information processing. Constructing a “rotational

magic trap” is the ideal solution to this problem. In such a laser trap, light-induced energy shifts of two or more rotational states are identical, eliminating dephasing associated with spatial variations in intensity across the trap.

The first guiding idea of selecting laser frequencies in the near-resonant region of forbidden transitions between the excited and ground states of the ultracold molecules was proposed and investigated in Ref. [1]. It was theoretically demonstrated that in such frequency intervals the light-induced decoherence is kept to a minimum. The further search for an efficient construction of the rotational magic traps for  $^{23}\text{Na}^{40}\text{K}$ ,  $^{87}\text{Rb}^{133}\text{Cs}$ , and  $^{23}\text{Na}^{87}\text{Rb}$  were pioneered by Refs. [2–4], respectively. Using a multi-configuration interaction approach the authors selected a laser frequency that has a small detuning (tens of GHz) relative to a narrow electronic transition between ground and excited electronic states. Close proximity to the forbidden transition poles allowed authors to significantly modify the trapping potentials for rotational levels of molecular ground states. At these laser frequencies rotational states experience the identical light shifts that significantly minimize the dephasing effect of spatially and temporal laser intensity fluctuations. Such a basic scheme can be readily applied to other molecules such as diatomic or related polyatomic molecules. However, using tweezer light that is tuned to a transition energy between hyperfine-resolved rovibrational levels of a ground and an excited electronic state is not always convenient as it can lead to unwanted scattering. Fortunately, tuning conditions can be relaxed when a static electric field is applied and the laser polarization direction or its ellipticity are carefully controlled relative to the quantization axis direction [5–11].

This paper focuses on quantitative theoretical mod-

\* skotoch@temple.edu

eling of dephasing and decoherence processes of ultracold NaRb molecules prepared in superpositions of rotational states and held in place by tweezer forces. First, we examine the dynamic real and imaginary polarizabilities of vibrationally cold polar  $^{23}\text{Na}^{87}\text{Rb}$  molecules as functions of the frequency of the trapping laser. Based on the knowledge of these polarizability values and accurate rovibrational transition energies between electronic ground and excited potentials, we determine magic tweezer frequencies where the following decoherence mechanisms, relevant to qubits encoded in rotational levels, are minimized. This dephasing is associated with spatial and temporal fluctuations of the laser intensity. In addition, we derive approximate analytical expressions for the dynamic polarizabilities in order to better understand the origin of magic conditions.

As a next step in improving the description of the polarizability of the  $^{23}\text{Na}^{87}\text{Rb}$  molecule, we studied the mixing of rotational levels of its  $v = 0$   $X^1\Sigma^+$  ground state in the presence of electric and magnetic fields as well as the trapping laser field. The anisotropy of the dynamic polarizability of rotational levels then manifests itself as a dependence on the orientation of the laser polarization relative to that of the electric field. Finally, our polar molecules have nonzero nuclear electric-quadrupole and nuclear-magnetic moments and the magnetic field further mixes states. The combined action of these three E&M fields is a powerful tool with which to manipulate and control ultracold molecules.

## II. MAGIC TRAPPING FREQUENCIES DUE TO $b^3\Pi_{0+}$ , $\nu' = 0$ RESONANCES

We begin by calculating the dynamic polarizability or ac Stark shift for rotational levels from  $J = 0$  to 5 of the  $v = 0$  vibrational level  $|X, vJM\rangle$  of the ground  $X^1\Sigma^+$  state of the  $^{23}\text{Na}^{87}\text{Rb}$  molecule absent external electric or magnetic fields and without molecular spin-rotation, hyperfine, and Zeeman interactions. Here,  $M$  is the projection quantum number of angular momentum  $J$  along a laboratory or space-fixed axis to be defined later on. The tweezer laser with laser frequency  $\nu$  is linearly polarized along space-fixed direction  $\vec{\epsilon}$  throughout this paper. We then determine laser light frequencies that allow simultaneous magic trapping of multiple rotational states using light nearly resonant with rovibrational levels of the  $b^3\Pi_{0+}$  state. Transitions between the  $X^1\Sigma^+$  and  $b^3\Pi_{0+}$  states are weak and only allowed through weak spin-orbit coupling with the  $A^1\Sigma_{0+}^+$  state.

Figure 1(a) schematically shows the NaRb molecule trapped in a tweezer potential, while Fig. 1(b) displays the three relevant relativistic  $\Omega = 0^+$  potential energy curves of the NaRb molecule, where  $\Omega$  is the absolute value of the projection quantum number of the total electronic angular momentum along the diatomic molecular axis. More precisely, the excited non-relativistic  $A^1\Sigma_{0+}^+$  and  $b^3\Pi_{0+}$  states are coupled by the spin-orbit interac-

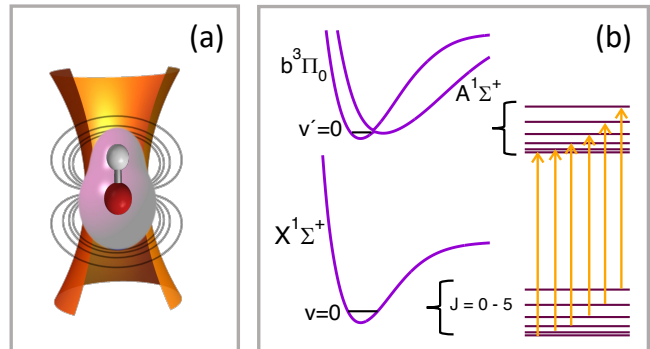


FIG. 1. (a) Schematic presentation of ground-state heteronuclear NaRb trapped in an optical tweezer potential. (b) The potential energies of the three most-important  $\Omega = 0^+$  electronic states of NaRb. The two black horizontal lines in the potentials represent the energetically lowest  $v = 0$  and  $v' = 0$  vibrational levels of the  $X^1\Sigma^+$  state and the  $A^1\Sigma^+$  and  $b^3\Pi_{0+}$  complex, respectively. Relevant rotational levels  $J = 0$  to 5 for both vibrational states are shown on the right. Near resonant optical transitions, orange lines with arrows, are used in a search for magic conditions as a function of tweezer laser frequency.

tion, which leads to  $\Omega = 0^+$  adiabatic potentials that have a narrow avoided crossing near interatomic separation  $R \approx R_c = 7.5a_0$  [12], where  $a_0$  is the Bohr radius. The energetically lowest  $\Omega = 0^+$  rovibrational states near the bottom or minimum of the nominally  $b^3\Pi_{0+}$  potential, however, have a small admixture of the  $A^1\Sigma_{0+}^+$  state. As electric dipole transitions between the  $X^1\Sigma^+$  and  $b^3\Pi_{0+}$  states are forbidden, this leads to weak, but easily observable transitions between to these  $\Omega = 0^+$  rovibrational levels of the ground electronic  $X^1\Sigma^+$  state. We observe that the equilibrium separations and harmonic frequencies of the  $X^1\Sigma^+$  and  $b^3\Pi_{0+}$  states are almost the same. We use the non-relativistic  $X^1\Sigma^+$ ,  $A^1\Sigma_{0+}^+$  and  $b^3\Pi_{0+}$  potentials, spin-orbit matrix elements, and the  $X^1\Sigma^+$  to  $A^1\Sigma^+$  electronic transition dipole moment as functions of  $R$  given by Refs. [12, 13].

For rotational states  $J, M$  of the  $v = 0$  ground-state of NaRb, the calculation of the sum over intermediate, excited states that appears in the evaluation of  $\alpha_{X, vJM}(\nu, \vec{\epsilon})$  can be simplified. The relevant laser frequencies are *nearly resonant* with rovibrational levels near the minimum of the  $b^3\Pi_{0+}$  potential. Consequently, we separate  $\alpha_{X, vJM}(\nu, \vec{\epsilon})$  into two contributions. The first contribution is due to these near-resonant transitions. We will use the rovibrational levels of this potential as well as corresponding vibrationally averaged transition dipole moments to construct the contribution to  $\alpha_{X, vJM}(\nu, \vec{\epsilon})$ . A second contribution to  $\alpha_{X, vJM}(\nu, \vec{\epsilon})$  is due to *off-resonant* transitions to other electronic states. They are computed within a quasi-static approximation where so-called parallel and perpendicular polarizabilities  $\alpha_{\parallel}(\nu, R)$  and  $\alpha_{\perp}(\nu, R)$ , corresponding to laser polarizations paral-

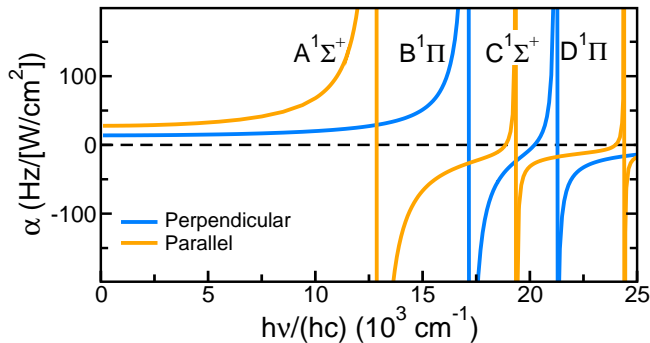


FIG. 2. The quasi-static parallel (orange curve) and perpendicular (blue curve) electronic polarizabilities of the  $X^1\Sigma^+$  state at its equilibrium separation  $R_e = 6.885a_0$  and photon energies up to  $hc \times 25000 \text{ cm}^{-1}$ . The energetically lowest four resonances are labeled with state  $^1\Lambda$ . The data is based on non-relativistic configuration-interaction calculations with the Q-Chem software package.

parallel and perpendicular relative to the body-fixed internuclear axis, respectively, are computed as functions of laser frequency and atom-atom separation  $R$  near the equilibrium separation  $R_e$  of the  $X^1\Sigma^+$  state using the linear response theory formulation within software package Q-Chem [14]. Q-Chem computes electronic states within a non-relativistic description of the electrons. In practice, we realize that these two quasi-static polarizabilities are to good approximation independent of  $R$  over the radial width of the  $v = 0$  vibrational level of the  $X^1\Sigma^+$  state. We thus only compute  $\alpha_{\parallel}(\nu, R)$  and  $\alpha_{\perp}(\nu, R)$  at  $R = R_e$  and drop argument  $R$  for the remainder of this article.

The two quasi-static polarizabilities of the  $X^1\Sigma^+$  state have been obtained with a non-relativistic configuration-interaction electronic-structure calculation using an all-electron basis set for Na. Single and double excitations were allowed from these basis functions. An effective core potential describes the 28 inner electrons of Rb. Single and double excitations were allowed for the remaining electrons of Rb.

Figure 2 shows the two quasi-static polarizabilities of the  $X^1\Sigma^+$  state of NaRb at  $R = R_e$  as functions of photon energy from zero to  $hc \times 25000 \text{ cm}^{-1}$ . Here,  $h$  is the Planck constant and  $c$  is the speed of light in vacuum. Over the large photon energy range shown in Fig. 2, several resonances are visible. Each corresponds to a transition between the  $X^1\Sigma^+$  state and a  $^1\Lambda$  state. In fact, in our non-relativistic formulation,  $\alpha_{\parallel}(\nu)$  only contains contributions from transitions to singlet  $^1\Sigma^+$  electronic states, while  $\alpha_{\perp}(\nu)$  only contains contributions from transitions to singlet  $^1\Pi$  states. Finally, we note that the quasi-static contributions to the polarizability of levels of the  $X^1\Sigma^+$  state have a small photon-energy dependence for photon energies near the minimum of the  $b^3\Pi_{0+}$  potential. The relevant quasi-static polarizabilities are off resonant.

The resonant contribution to the polarizability has

been determined in several steps. We compute two-channel radial eigenvalues and eigenfunctions of the spin-orbit coupled and shifted  $\Omega = 0^+$   $A^1\Sigma^+$  and  $b^3\Pi_{0+}$  states for total angular momentum  $J' = 0, 1, \dots, 6$  using a discrete variable representation (DVR) of the radial relative kinetic energy operator [15]. For each  $J'$ , the eigenvalues  $E_{Ab,v'J'}$  are labeled  $v' = 0, 1, \dots$  with increasing energy and wavefunctions of the energetically lowest  $v'$  levels are to good approximation  $b^3\Pi_{0+}$  states. The energies are independent of projection quantum number  $M'$  of  $J'$ .

We then compute rovibrational wavefunctions  $v$  and energies  $E_{X,vJ}$  of the  $X^1\Sigma^+$  state for  $J$  up to 5 with the same DVR and radial grid used to compute eigenpairs of the coupled  $A^1\Sigma^+$  and  $b^3\Pi_{0+}$  system. The energies are independent of projection quantum number  $M$  of  $J$ . The use of the same radial grid avoids interpolation of wavefunctions in the computation of vibrationally-averaged transition dipole moments using the  $R$ -dependent transition dipole moment between the  $X^1\Sigma^+$  and  $A^1\Sigma^+$  states.

Finally, we compute the resonant-part of the polarizability  $\alpha_{X,vJM}(\nu, \vec{\epsilon})$  of  $v = 0, JM$   $X^1\Sigma^+$  states using only the energetically lowest rovibrational levels of the coupled  $A^1\Sigma^+ - b^3\Pi_{0+}$  system that have a large  $b^3\Pi_{0+}$  character and thus a small vibrationally-averaged transition dipole moment. The choice to limit the determination of the resonant-part of the polarizability to a few levels of the  $A^1\Sigma^+ - b^3\Pi_{0+}$  system avoids double counting the effects of the  $A^1\Sigma^+$  state when combining the resonant and off resonant contributions of  $\alpha_{X,vJM}(\nu, \vec{\epsilon})$ . In principle, the projection degeneracy is broken by hyperfine interactions between nuclear quadrupole moments and the rotation of the molecule as well as Zeeman interactions for the nuclear spins. The nuclear spin of both  $^{23}\text{Na}$  and  $^{87}\text{Rb}$  is  $3/2$ . However, the hyperfine splittings for the  $\Omega = 0^+$  states are small Ref. [16] compared to the rotational energies described below. Here, we omit the effects of hyperfine interactions on magic conditions.

Figure 3 shows dynamic polarizabilities of the  $v = 0, J = 0, 1, \dots, 5$ , and  $M = 0$ , rotational levels of the  $^{23}\text{Na}^{87}\text{Rb}$   $X^1\Sigma^+$  state absent an external electric field but with a 335 Gauss magnetic field parallel to the linearly polarized light as functions of laser frequency in the neighborhood of the  $v' = 0$  level of the coupled  $A^1\Sigma^+ - b^3\Pi_0$  system. The dynamic polarizabilities include both the resonant and off-resonant contributions. The horizontal axis gives photon energy detuning  $\Delta = h\nu - \mathcal{E}_{v'=0}$ , where molecular transition energy  $\mathcal{E}_{v'=0} = E_{Ab,v'=0,J'=1} - E_{X,v=0,J=0}$ . Our estimate provides that  $\mathcal{E}_{v'=0} = hc \times 11306.4 \text{ cm}^{-1}$ , which corresponds to a laser wavelength close to 884 nm. We chose the quantization axis of the molecular angular momentum  $J$  and  $J'$  in the same direction as that of the laser polarization.

The curves for  $J = 0$  and  $J > 0$  in Fig. 3 have different behaviors. The polarizability for the  $J = 0$  has a single resonance at  $\Delta = 0$ . Those for  $J > 0$  have two resonances located at  $L_J(v = 0, v' = 0)$  and  $R_J(v = 0, v' = 0)$ , where

$$L_J(v, v') = J(J+1)B_v - [J(J-1) - 2]B_{v'} \quad (1)$$

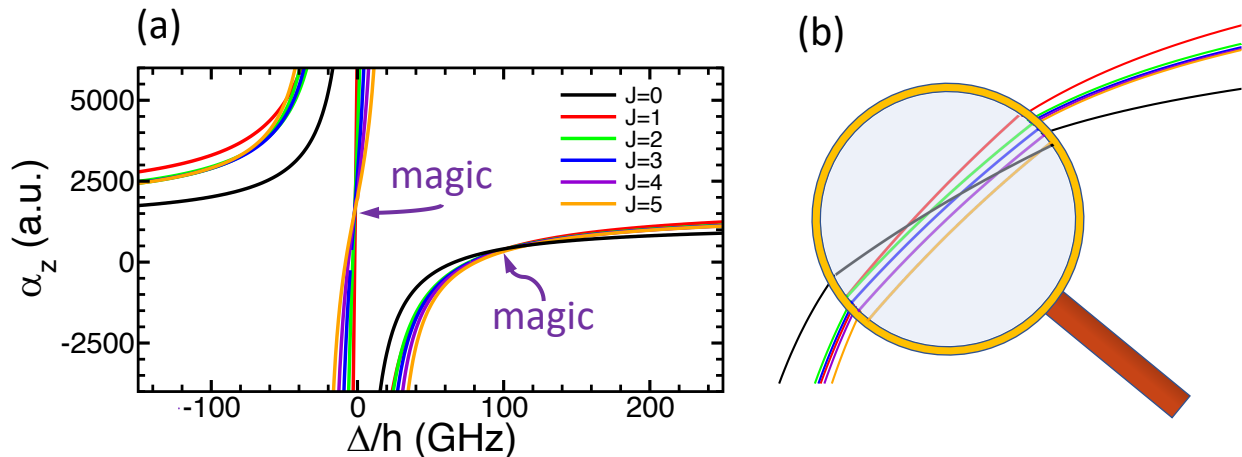


FIG. 3. (a)  $^{23}\text{Na}^{87}\text{Rb}$  dynamic polarizabilities of rotational  $v = 0$  levels of the  $X^1\Sigma^+$  state in atomic units for  $z$ -linear polarized light as functions of laser frequency detuning  $\Delta/h$  near transitions from the  $v = 0$   $X^1\Sigma^+$  state to the  $v' = 0$  level of the coupled  $A^1\Sigma^+-b^3\Pi_0$  system. Each curve corresponds to the dynamic polarizability of a different rotational level  $J$  with  $M = 0$ . Zero detuning  $\Delta$  corresponds to the resonant transition from  $v = 0, J = 0$  level of the  $X^1\Sigma^+$  state to the  $v' = 0, J' = 1$  level of the coupled  $A^1\Sigma^+-b^3\Pi_0$  system. The purple arrows indicate magic detunings, where multiple rotational states have the same or nearly the same polarizabilities. (b) Schematically magnified region of dynamic polarizabilities, near the frequency detuning  $\Delta/h = 100$  GHz. The colors of the curves are the same as those in panel (a). We observe that the curve for  $J = 0$  crosses those for  $J > 0$ .

and

$$R_J(v, v') = J(J+1)B_v - [(J+1)(J+2) - 2]B_{v'} \quad (2)$$

with rotational constants  $B_v$  and  $B_{v'}$  for the  $v$  vibrational level of the  $X^1\Sigma^+$  state and the  $v' = 0$  vibrational level of the coupled  $A^1\Sigma^+-b^3\Pi_0$  system, respectively. For  $^{23}\text{Na}^{87}\text{Rb}$ ,  $B_{v=0}/hc = 0.06970 \text{ cm}^{-1}$  and  $B_{v'=0}/hc = 0.06988 \text{ cm}^{-1}$ . The two values agree to better than 0.5%. These behaviors follow from photon selection rules  $|J-1| \leq J' \leq J+1$  and  $J'-J$  is odd.

Panel (a) of Fig. 3 shows that there exist two *magic* laser frequencies. The first is located near  $\Delta/h = -2$  GHz and  $J > 0$  rotational levels have nearly the same polarizabilities. The second is located near  $\Delta/h = 100$  GHz, all  $J = 0, \dots, 5$  rotational levels have nearly the same polarizabilities. Panel (b) looks in more detail at the latter frequency region. In particular, the polarizability of the  $J = 0$  level is equal to that of the  $J = 1, 2, 3, 4, 5$  rotational levels at detuning  $\Delta/h = 103$  GHz, 105 GHz, 108 GHz, 112 GHz, and 116 GHz, respectively. In fact, the differences between these  $\Delta$  with  $J > 0$  is increasing with  $J$ . The origin of this effect lies in the increase of rotational energies with  $J$ .

### III. ANALYTICAL RESULTS FOR MAGIC POLARIZABILITY

We find it useful to derive analytical expression for the dynamic polarizabilities shown in Fig. 3 in order to better understand the origin of magic conditions as well as simplifying their determination for wide variety of molecules. For rovibrational level  $v = 0$   $JM$  of the  $X^1\Sigma^+$  state, the dynamic polarizability for linearly-polarized laser light near transitions to vibrational states  $v' = 0$  or  $v' = 1$  of the coupled  $A^1\Sigma^+-b^3\Pi_0$  system is well approximated by

$$\alpha_{X,v=0JM}(\nu, \vec{\epsilon}) = -\frac{3\pi c^2}{2\omega_{v'}^3} \left[ A_{J,M}(\theta_p) \frac{\hbar\Gamma_{0,v'}}{\Delta_{v'} + L_J(0, v')} \right. \\ \left. + B_{J,M}(\theta_p) \frac{\hbar\Gamma_{0,v'}}{\Delta_{v'} + R_J(0, v')} \right] \\ + [A_{J,M}(\theta_p) + B_{J,M}(\theta_p)] (\alpha_{\text{bg},\parallel} - \alpha_{\text{bg},\perp}) + \alpha_{\text{bg},\perp}, \quad (3)$$

where  $\theta_p$  is the angle between the polarization of the laser  $\vec{\epsilon}$  with respect to the quantization axis for the molecular states, our laboratory-fixed  $z$  axis. The energy detuning

$$\Delta_{v'} = h\nu - \hbar\omega_{v'} \quad (4)$$

with  $\hbar\omega_{v'} = E_{\text{Ab},v',J'=1} - E_{\text{X},v=0,J=0}$ . The terms on the first two lines of Eq. (3) lead to resonances in the dynamic polarizability. In fact, there are one and two resonances for  $J = 0$  and  $J > 0$ , respectively. The  $\Gamma_{0,v'}$

are linewidths of the vibrational levels  $v'$  of the coupled  $A^1\Sigma^+-b^3\Pi_{0+}$  system.

The parallel and perpendicular  $\alpha_{\text{bg},\parallel}$  and  $\alpha_{\text{bg},\perp}$  are body-fixed background polarizabilities. The dimensionless angular factor  $A_{J,M}(\theta_p)$  is given by

$$A_{J,M}(\theta_p) = \frac{J(J+1) - 3M^2}{2(2J+1)(2J-1)} \cos^2 \theta_p \quad (5)$$

$$+ \frac{(J-1)J + M^2}{2(2J+1)(2J-1)}$$

for  $|M| < J$  and

$$A_{J,M}(\theta_p) = \frac{(J+|M|)(J+|M|-1)}{4(2J+1)(2J-1)} \sin^2 \theta_p \quad (6)$$

for  $|M| = J$ . Note that  $A_{J,M}(\theta_p) = 0$  for  $J = 0$ . Finally, the dimensionless  $B_{J,M}(\theta_p)$  is given by

$$B_{J,M}(\theta_p) = \frac{J(J+1) - 3M^2}{2(2J+1)(2J+3)} \cos^2 \theta_p \quad (7)$$

$$+ \frac{(J+1)(J+2) + M^2}{2(2J+3)(2J+1)}.$$

Equation (3) can only be used for energy detunings that are much smaller than the vibrational spacing between different  $v'$  states of the  $A^1\Sigma^+-b^3\Pi_{0+}$  system. On the other hand, the energy detunings must be much larger than any hyperfine and Zeeman splittings in the coupled  $A^1\Sigma^+-b^3\Pi_{0+}$  system and for energy detunings much larger than  $\hbar\Gamma_{0,v'}$ .

Finally, a Taylor expansion of the right hand side of Eq. (3) assuming  $|\Delta_{v'}| \gg |L_J|$  and  $|\Delta_{v'}| \gg |R_J|$  gives

$$\alpha_{X,v=0JM}(\nu, \vec{\epsilon}) = [A_{J,M}(\theta_p) + B_{J,M}(\theta_p)] \quad (8)$$

$$\times \left( -\frac{3\pi c^2 \hbar \Gamma_{0,v'}}{2\omega_{v'}^3 \Delta_{v'}} + \alpha_{\text{bg},\parallel} - \alpha_{\text{bg},\perp} \right) + \alpha_{\text{bg},\perp} + \dots$$

From an inspection of Eq. (8), we realize that we can always find an energy detuning independent of  $\theta_p$  and  $J$  such that the term in parenthesis vanishes. At this energy detuning the dynamic polarizability is  $\alpha_{\text{bg},\perp}$ , the same for all  $\theta_p$  and  $J$  within our approximations, and the optical trap is magic for all rotational states. Higher-order terms in Eq. (8) will add small  $\theta_p$ - and  $J$ -dependent corrections and are observed in Fig. 3.

#### IV. VIBRATIONALLY-RESOLVED IMAGINARY POLARIZABILITIES OF THE $X^1\Sigma^+$ STATE

In addition, we developed an approach based on ideas of Refs. [1] to evaluate the imaginary dynamic polarizabilities of rovibrational levels of the ground state in vicinity of rovibrational levels of the excited state potentials. The imaginary part of  $\alpha_i$  describes incoherent decay that leads to loss of molecules from the optical trap. Our calculation is based on perturbation theory method with specific focus on relativistic spin-orbit

coupling between  $A^1\Sigma^+-b^3\Pi_0$  complex. The simulations are performed using electronic potentials, permanent, and transition dipole moments of NaRb determined in Refs. [12, 13, 17].

We analyze the imaginary dynamic polarizability in the wide range laser frequency from 10000 to 20000  $\text{cm}^{-1}$  that is in the resonance with multiple vibrational levels of the excited state potentials.

The molecular dynamic  $\alpha_i(\hbar\nu, \vec{\epsilon})$  at frequency  $\nu$  and laser polarizability  $\vec{\epsilon}$  of state  $i$  is complex valued. To good approximation its imaginary part is

$$\text{Im}[\alpha(\hbar\nu, \vec{\epsilon})] = -\frac{1}{\epsilon_0 c} \sum_f \frac{\hbar\gamma_f/2}{(E_f - E_i)^2 - (\hbar\nu)^2} \quad (9)$$

$$\times |\langle f|d(R)\hat{R} \cdot \vec{\epsilon}|i\rangle|^2,$$

where kets  $|i\rangle$  and  $|f\rangle$  are simplified labels for initial rovibrational wavefunctions of the  $X^1\Sigma^+$  potential and those of excited electronic states, respectively. Their energies are  $E_i$  and  $E_f$ , respectively, and  $\gamma_f$  is the natural line width of excited rovibrational levels.

Figure 4, panels (a), (b), and (c) demonstrate imaginary dynamic polarizabilities of the  $J = 0, 1$ , and 2 rotational levels, respectively, of  $X^1\Sigma^+$  with projection quantum number  $M = 0$ . It turns out that, to good approximation, the three curves are the same except for a frequency-independent scale factor. Deviations from these scalings occur very close to the resonances, i.e. on the order of the rotational spacing of the molecule. We calculate imaginary polarizabilities for these levels taking into account the rovibrational structure of lower excited states in the units of  $\text{MHz}/[\text{W}/\text{cm}^2]$ , which are often used in experimental measurements. Note that one atomic unit of polarizability corresponds to  $4.68645 \times 10^{-8} \text{ MHz}/[\text{W}/\text{cm}^2]$ .

We evaluated the rovibrational molecular line widths of excited electronic states dissociating to either a singly-excited Na or Rb atom by first computing a  $R$ -dependent optical potential  $-i\Gamma(R)/2$  [18] for each excited electronic state. Here,  $\Gamma(R)$  is positive and proportional to  $|\delta E(R)|^3 d^2(R)$ , where  $\delta E(R)$  and  $d(R)$  at internuclear separation  $R$  are the potential energy difference and the transition electronic dipole moment between an excited state and the ground state, respectively. Finally, the energies  $E_i$  and  $E_f$  and line widths  $\gamma_f$  of rovibrational levels of electronic states were found by computing radial rovibrational wavefunctions, energies, and matrix elements of  $\Gamma(R)$ . By construction, the imaginary part is negative. Its value is seven orders of magnitude smaller than the real part. For  $J = 1$  and 2,  $M = 0$  the polarizability depends on the polarization direction of the trapping light.

The imaginary part of the polarizabilities are slowly varying with frequency in regions outside multiple closely spaced resonant features, where  $\alpha(\hbar\nu, \vec{\epsilon})$  is orders of magnitude larger than in the slowly varying regions. The resonant like features are due to the rovibrational bound states of excited electronic potentials. In fact, we could

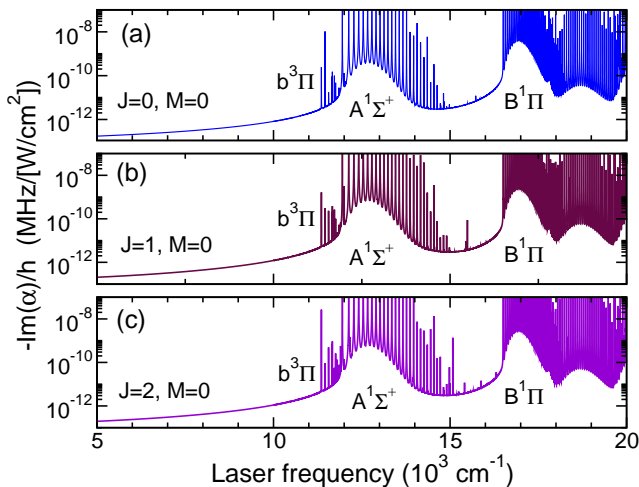


FIG. 4. Minus one times the imaginary part of the dynamic polarizabilities of the  $J = 0, 1,$  and  $2$  rotational levels of the vibrational ground state of  $^{23}\text{Na}^{87}\text{Rb}$  with projection quantum number  $M = 0$  along the  $z$  axis as functions of laser frequency in panels (a), (b), and (c), respectively. Imaginary polarizabilities are presented for laser polarization  $\sigma_s$  along the  $\vec{z}$  directions.

assign the resonances as due to the  $b^3\Pi$ ,  $A^1\Sigma^+$ , and  $B^1\Pi$  states. These resonances are strongest when the inner- or outer-turning point of rovibrational wavefunctions of the excited electronic potentials coincides with the equilibrium separation of the  $X^1\Sigma^+$  potential.

The calculations of the imaginary part of the polarizability allowed us predict the role of unwanted decoherence processes. In particular, optical fields can transfer population from a rovibrational level of the electronic ground state to rovibrational levels of an excited electronic state, which then by the spontaneous emission decays to many rovibrational levels of the  $X^1\Sigma^+$  state. As a result, we lose control over the molecule.

### EFFECT OF EXTERNAL ELECTRIC FIELD ON THE MAGIC CONDITION

We extended the ideas of Refs. [11] and simulated the rovibrational and hyperfine quantum states of  $^{23}\text{Na}^{87}\text{Rb}$  molecules when both a magnetic field  $\vec{B}$  and electric field  $\vec{E}$  are present at a fixed laser wavelength of  $\lambda = 1064$  nm or wavenumber of  $E/hc \approx 9400$   $\text{cm}^{-1}$ . For the  $X^1\Sigma^+$  electronic state hyperfine effects are due to the nuclear spins of the atoms. Understanding the effect of changing the relative orientation or polarization of the E&M fields is of crucial importance for the creation of decoherence-free sub-spaces built from two or more rovibrational and hyperfine states. The effective Hamiltonian for the  $v = 0$  rotational-hyperfine levels of the  $X^1\Sigma^+$  state of  $^{23}\text{Na}^{87}\text{Rb}$  is obtain using the formalism developed in our previous studies [3, 6, 7].

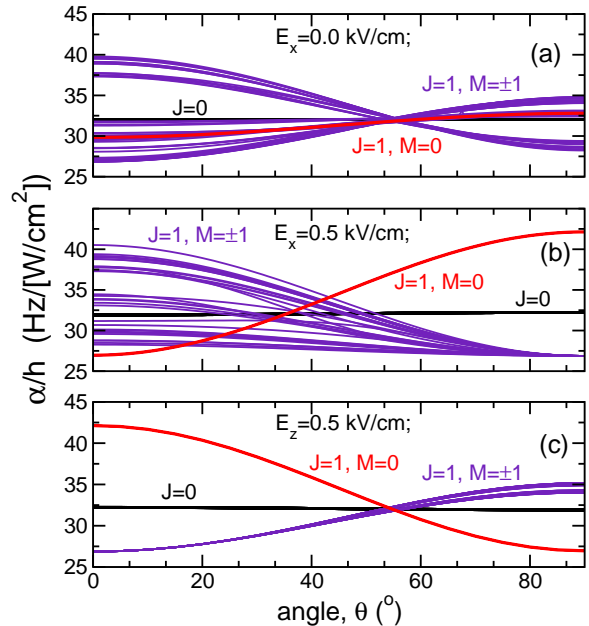


FIG. 5. Dynamic polarizabilities of all  $J = 0$  and  $1$  hyperfine eigenstates of  $v = 0$   $X^1\Sigma^+$   $^{23}\text{Na}^{87}\text{Rb}$  as functions of the angle  $\theta$  between the linear laser polarization and a space-fixed  $z$  axis, when the nuclear quadrupole interaction is present and a magnetic of  $335.6$  G is applied along the  $z$  axis at a fixed laser wavelength of  $\lambda = 1064$  nm or wavenumber of  $E/hc \approx 9400$   $\text{cm}^{-1}$ . Panels (a), (b), and (c) show polarizabilities for an electric field of  $0.0$  kV/cm and  $0.5$  kV/cm applied along the  $x$  and the  $z$  axis. Black and red curves correspond to hyperfine states with dominant  $J = 0, M = 0$  and  $J = 1, M = 0$  character, respectively. Purple curves correspond to hyperfine states with  $J = 1, M = \pm 1$  character.

We computed the eigenenergies  $\mathcal{E}_i$  of  $H$  including the lowest  $J = 0$  and  $J = 1$  rotational states of our molecule for many relative orientations of  $\vec{B}$ ,  $\vec{E}$ , and  $\vec{e}$  as well as the magnitudes of  $\vec{B}$  and  $\vec{E}$  and intensity  $I_{\text{trap}}$ . For the physically relevant  $B$ ,  $E$ , and  $I_{\text{trap}}$ , the energy shifts due to the Zeeman, electric-dipole, nuclear quadrupole, and polarization interactions are much smaller than those due to the  $B_{v=0}\vec{J}^2$  rotational interaction. Without an electric field nuclear spin states mix with the three projections of  $J = 1$  and the polarizabilities of these eigenstates differ significantly from each other.

Figure 5 shows the dynamic polarizabilities of the lowest 64 eigenstates of  $v = 0$   $X^1\Sigma^+$   $^{23}\text{Na}^{87}\text{Rb}$ , corresponding to all nuclear hyperfine states of  $J = 0$  and  $1$  rotational states, as functions of the angle  $\theta$  between the linear laser polarization and a space-fixed  $z$  axis. The laser intensity is  $I_{\text{trap}} = 2$  kW/cm. There is magnetic field of  $335.6$  G along the  $z$  present. Panel (a) shows data for an electric field of  $0.0$  kV/cm. whereas panels (b) and (c) show an electric field value is  $0.5$  kV/cm oriented along  $x$  and  $z$  axis, respectively. In all three panels the polarizabilities have been obtained including quadrupole cou-

plings between nuclear spins and the molecular rotation. In panel (c) the dynamic polarizability of  $J = 1, M = 0$  hyperfine states coalesce into a single curve. Those for  $M = \pm 1$  states still have a complex dependence on hyperfine states. Near Feshbach resonances atom pairs can be associated into weakly-bound  $^{23}\text{Na}^{87}\text{Rb}$  molecules with time-dependent magnetic field ramps. In fact, the polarizabilities of  $J = 0, M = 0$  and  $J = 1, M = 0$  states are equal for  $\theta \approx 55^\circ$ , a magic condition. The  $M = +1$  and  $M = -1$  degeneracy of  $J = 1$  eigenstates, however, is lifted and eigenstates are labeled as either  $M = -1$  or

1.

In our formalism we include the nuclear quadrupole interaction  $H_Q = \sum_k (eqQ)_k (C_2(\alpha, \beta) \cdot T_2(\vec{v}_k, \vec{v}_k)) / [i_k(i_k - 1)]$  with one contribution for each atom. It has strengths  $(eqQ)_k$  and couples nuclear spins to rotational states  $J$ . Here,  $C_{2m}(\alpha, \beta)$  is a spherical harmonic function that depends on angle  $\alpha$  and  $\beta$  orienting the molecular axis and  $T_{2m}(\vec{v}_k, \vec{v}_k)$  is a rank-2 spherical tensor constructed from spin  $\vec{v}_k$ . For  $^{23}\text{Na}^{87}\text{Rb}$ , the parameters  $(eqQ)_k$  were first given in Ref. [19] as  $(eqQ)_{\text{Na}}/h = 0.132$  MHz and  $(eqQ)_{\text{Rb}}/h = -2.984$  MHz. Finally, the polarization interaction

$$H_{\text{pol}} = -\frac{1}{3} [\alpha_{\parallel}(\nu) + 2\alpha_{\perp}(\nu)] I_{\text{trap}} - \frac{\sqrt{6}}{3} [\alpha_{\parallel}(\nu) - \alpha_{\perp}(\nu)] T_2(\vec{\epsilon}, \vec{\epsilon}) \cdot C_2(\alpha, \beta) I_{\text{trap}}, \quad (10)$$

where  $I_{\text{trap}}$  is the intensity of the trapping laser. The rank-2 tensor operators in  $H_{\text{pol}}$  capture its dependence on (linear) laser polarization  $\vec{\epsilon}$  and rotational state of the molecule [5]. The Hamiltonian  $H_{\text{pol}}$  involves the frequency-dependent  $v = 0$  vibrationally-averaged parallel and perpendicular polarizabilities, which for  $^{23}\text{Na}^{87}\text{Rb}$  are  $\alpha_{\parallel}/h = 57.904$  Hz/(W/cm<sup>2</sup>) and  $\alpha_{\perp}/h = 19.079$  Hz/(W/cm<sup>2</sup>) at a laser wavelength of 1064 nm. Typically, the laser intensity  $I_{\text{trap}}$  is of order 1 kW/cm<sup>2</sup>. We neglect contributions from centrifugal distortions, the rotational Zeeman interaction, and other hyperfine terms.

## CONCLUSION

In this paper we developed a theoretical approach to construct an optical trap for a single NaRb molecule where molecular rotational-hyperfine states have so called magic conditions. Constructing a rotational magic trap is the ideal solution the long rotational coherence times needed to exploit the rotational degree of freedom as the quantum bit in quantum information processing. In such a laser trap, light-induced energy shifts of multiple rotational states of the ground configuration are the same, eliminating dephasing associated with spatial variations in intensity across the trap. This opens up the prospect of using the rotational degree of freedom of the molecule to encode a synthetic dimension in addition to having multiple molecule-containing traps in real space.

We used several ways to reach this goal: a) changing a trapping laser frequency in the region that close to or in between the narrow transitions from  $v = 0, J = 0$  of the  $X^1\Sigma^+$  state to the  $v' = 0$  and  $v' = 1$  vibrational levels of

the spin-orbit coupled  $A^1\Sigma^+ - b^3\Pi_0$  complex. No external electric field is present. The magnetic field strength is 335.6 G; b) changing field orientation relative to polarization of trapping light with magnetic field of 335.6 G is on and a static electric field is on and off.

For case a), we predict nearly magic conditions for the lowest six rotational states of the  $v = 0$  level at detuning  $\Delta/h = -2$  GHz and 100 GHz from the  $v'=0, J' = 1$  level of the  $b^3\Pi_0$  potential. Case b) focuses on finding the magic conditions taking into account the nonzero nuclear spins of  $^{23}\text{Na}$  and  $^{87}\text{Rb}$ , which align along the magnetic field through the Zeeman interaction. Moreover, nuclear quadrupole interactions mix nuclear spin states with the rotation of the molecule. This causes the rotating molecules to dephase quickly in the inhomogeneous trapping laser field. This dephasing can be canceled to first order by selecting a specific angle between the angular momentum of the molecule  $J$  and the trapping field polarization direction such that the differential polarizability vanishes. We have shown that applying an electric field along the magnetic field direction decouples the hyperfine states and thus reduces second-order differential light shifts.

## ACKNOWLEDGEMENTS

Our research is supported by the U.S. Air Force Office of Scientific Research Grants No. FA9550-19-1-0272. Work at Temple University is also supported by the U.S. Air Force Office of Scientific Research Grants No. FA9550-21-1-0153 and the NSF Grant No. PHY-1908634.

[1] Kotochigova, S.; Tiesinga, E. Controlling polar molecules in optical lattices. *Phys. Rev. A* **2006**, *73*, 041405(R).

[2] Bause, R.; Li, M.; Schindewolf, A.; Chen, X.-Y.; Duda, M.; Kotochigova, S.; Bloch, I.; Luo, X.-Y. Tune-

- Out and Magic Wavelengths for Ground-State  $^{23}\text{Na}^{40}\text{K}$  Molecules. *Phys. Rev. Lett.* **2020**, *125*, 023201.
- [3] Guan, Q.; Cornish, S. L.; Kotochigova, S. Magic conditions for multiple rotational states of alkali molecules in optical lattices. *Phys. Rev. A* **2021**, *103*, 043311.
- [4] He, J.; Lin, J.; Vexiau, R.; Bouloufa-Maafa, N.; Dulieu, O.; Wang, D. Characterization of the lowest electronically excited-state ro-vibrational level of  $^{23}\text{Na}^{87}\text{Rb}$ . *New J. Phys.* **2021**, *23*, 115003.
- [5] Kotochigova, S.; DeMille, D. Electric-field-dependent dynamic polarizability and state-insensitive conditions for optical trapping of diatomic polar molecules. *Phys. Rev. A* **2010**, *82*, 063421.
- [6] Petrov, A.; Makrides, C.; Kotochigova, S. External field control of spin-dependent rotational decoherence of ultracold polar molecules. *Mol. Phys.* **2013**, *111*, 1731–1737.
- [7] Neyenhuis, B.; Yan, B.; Moses, S. A.; Covey, J. P.; Chotia, A.; Petrov, A.; Kotochigova, S.; Ye, J.; Jin, D. S. Anisotropic Polarizability of Ultracold Polar  $^{40}\text{K}^{87}\text{Rb}$  Molecules. *Phys. Rev. Lett.* **2012**, *109*, 230403.
- [8] Rosenbrand, T.; Grimes, D. D.; Ni, K.-K. Elliptical polarization for molecular Stark shift compensation in deep optical traps. *Opt. Express* **2018**, *26*, 19821–19825.
- [9] Blackmore, J. A.; Caldwell, L.; Gregory, P. D.; Bridge, E. M.; Sawant, R.; Aldegunde, J.; Mur-Petit, J.; Jaksch, D.; Hutson, J. M.; Sauer, B. E.; Tarbutt, M. R.; Cornish, S. L. Ultracold molecules for quantum simulation: rotational coherences in CaF and RbCs. *Quantum Science and Technology* **2018**, *4*, 014010.
- [10] Blackmore, J. A.; Sawant, R.; Gregory, P. D.; Bromley, S. L.; Aldegunde, J.; Hutson, J. M.; Cornish, S. L. Controlling the ac Stark effect of RbCs with dc electric and magnetic fields. *Phys. Rev. A* **2020**, *102*, 053316.
- [11] Lin, J.; He, J.; Ye, X.; Wang, D. Anisotropic polarizability of ultracold ground-state  $^{23}\text{Na}^{87}\text{Rb}$  molecules. *Phys. Rev. A* **2021**, *103*, 023332.
- [12] Docenko, O.; Tamanis, M.; Ferber, R.; Pazyuk, E. A.; Zaitsevskii, A.; Stolyarov, A. V.; Pashov, A.; Knöckel, H.; Tiemann, E. Deperturbation treatment of the  $A^1\Sigma^+ - b^3\Pi$  complex of NaRb and prospects for ultracold molecule formation in  $X^1\Sigma^+(v=0; J=0)$ . *Phys. Rev. A* **2007**, *75*, 042503.
- [13] Pashov, A.; Docenko, O.; Tamanis, M.; Ferber, R.; Knöckel, H.; Tiemann, E. Second-quantized formulation of geometric phases. *Phys. Rev. A* **2005**, *72*, 012111.
- [14] Shao, Y.; *et al.*, Advances in molecular quantum chemistry contained in the Q-Chem 4 program package. *Molecular Physics* **2015**, *113*, 184–215.
- [15] Colbert, D. T.; Miller, W. H. A novel discrete variable representation for quantum mechanical reactive scattering via the S-matrix Kohn method. *J. Chem. Phys.* **1992**, *96*, 1982–1991.
- [16] Zhu, B.; Li, X.; He, X.; Guo, M.; Wang, F.; Vexiau, R.; Bouloufa-Maafa, N.; Dulieu, O.; Wang, D. Long-range states of the NaRb molecule near the  $\text{Na}(3^2S_{1/2}) + \text{Rb}(5^2P_{3/2})$  asymptote. *Phys. Rev. A* **2016**, *93*, 012508.
- [17] R. Vexiau, D. B.; Lepers, M.; Orbán, A.; Aymar, M.; Dulieu, O.; Bouloufa-Maafa, N. Dynamic dipole polarizabilities of heteronuclear alkali dimers: optical response, trapping and control of ultracold molecules. *International Reviews in Physical Chemistry* **2017**, *36*, 709–750.
- [18] Zygelman, B.; Dalgarno, A. Radiative quenching of  $\text{He}(2^1S)$  induced by collisions with ground-state helium atoms. *Phys. Rev. A* **1988**, *38*, 1877–1884.
- [19] Aldegunde, J.; Hutson, J. M. Hyperfine structure of alkali-metal diatomic molecules. *Phys. Rev. A* **2017**, *96*, 042506.